

Published in final edited form as:

Nat Commun. 2014 ; 5: 3309. doi:10.1038/ncomms4309.

Lipidic cubic phase injector facilitates membrane protein serial femtosecond crystallography

Uwe Weierstall¹, Daniel James¹, Chong Wang², Thomas A. White⁷, Dingjie Wang¹, Wei Liu², John C.H. Spence¹, R. Bruce Doak¹, Garrett Nelson¹, Petra Fromme³, Raimund Fromme³, Ingo Grotjohann³, Christopher Kupitz³, Nadia A. Zatsepin¹, Haiguang Liu¹, Shibom Basu³, Daniel Wacker², Gye Won Han², Vsevolod Katritch², Sébastien Boutet⁴, Marc Messerschmidt⁴, Garth J. Williams⁴, Jason E. Koglin⁴, M. Marvin Seibert^{4,5}, Markus Klinker^{6,7}, Cornelius Gati⁷, Robert L. Shoeman⁸, Anton Barty⁷, Henry N. Chapman^{7,9,10}, Richard A. Kirian^{1,7}, Kenneth R. Beyerlein⁷, Raymond C. Stevens², Dianfan Li¹¹, Syed T.A. Shah¹¹, Nicole Howe¹¹, Martin Caffrey¹¹, and Vadim Cherezov²

¹Department of Physics, Arizona State University, Tempe AZ 85287, USA ²Department of Integrative Structural and Computational Biology, The Scripps Research Institute, La Jolla, CA 92037, USA ³Department of Chemistry and Biochemistry, Arizona State University, Tempe AZ 85287, USA ⁴SLAC National Accelerator Laboratory, 2575 Sand Hill Road, Menlo Park, CA 94025 ⁵Laboratory of Molecular Biophysics, Department of Cell and Molecular Biology, Uppsala University, Husargatan 3 (Box 596), SE-751 24 Uppsala, Sweden ⁶Departamento de Química, Universidad Autónoma de Madrid, Ciudad Universitaria de Cantoblanco, 28049 Madrid ⁷Center for Free-Electron Laser Science, Notkestrasse 85, 22607 Hamburg, Germany ⁸Max-Planck-Institut für medizinische Forschung, Jahnstrasse 29, 69120 Heidelberg, Germany ⁹Institute for Experimental Physics, University of Hamburg, 22761 Hamburg, Germany ¹⁰Center for Ultrafast

Corresponding authors: Uwe Weierstall (weier@asu.edu) and Vadim Cherezov (vcherezo@scripps.edu).

Author Contributions

U.W. invented and designed the LCP injector and wrote the manuscript; operation of the sample delivery system was performed by U.W., D.J., Di.W., Ch. K., G.N.; W.L. developed microcrystal sample preparation in LCP protocol, prepared samples, assisted in testing the LCP injector, data collection and manuscript preparation; J.C.H.S. contributed to the development of the injector and the Monte Carlo method; R.B.D. contributed to the design of the LCP injector; P.F. was involved in the initiation and planning of the experiments, assisted with sample characterization, data collection and contributed to writing the paper; R.F., Ch.K., I.G. participated in data collection and contributed to sample characterization; N.A.Z., Sh.B., C.G. participated in data collection, processed and analyzed data; H.L. helped with data analysis; Da.W. prepared GPCR microcrystals in LCP and helped with data collection; C.W. prepared SMO/cyclopamine microcrystals in LCP; T.A.W. analyzed the SMO/cyclopamine data, G.W.H. refined the SMO/cyclopamine structure, V.K. analyzed the structure and cyclopamine binding pose; Sé.B., M.M., G.J.W., J.E.K., M.M.S. setup the x-ray FEL experiment, beamline, controls and data acquisition, operated the CXI beamline and performed the data collection; R.L.S. contributed to the design and operation of the LCP injector and delivery system, and read and revised manuscript; A.B. participated in data collection, wrote data processing software and helped with data processing and with writing the paper; H.N.C. supervised software development and data processing, helped with writing the paper; R.A.K. developed the Monte Carlo integration method, contributed to data processing; K.R.B. and M.K. contributed to software development and data processing; R.C.S. supervised GPCR production and contributed to writing the manuscript; D.L. and N.H. produced and crystallized DgkA; D.L. helped with data collection; S.T.A.S. synthesized and purified 7.9 MAG; M.C. supervised the DgkA and 7.9 MAG synthesis and purification work, helped with data collection and with writing the paper; V.C. conceived the project, designed the experiments, supervised data collection, analyzed the results and wrote the manuscript.

Competing Financial Interests:

The authors declare no competing financial interests.

The coordinates and structure factors have been deposited in the Protein Data Bank under the accession code 4O9R.

Imaging, 22607 Hamburg, Germany ¹¹School of Medicine and School of Biochemistry and Immunology, Trinity College, Dublin, Dublin 2, Ireland

Abstract

Lipidic cubic phase (LCP) crystallization has proven successful for high-resolution structure determination of challenging membrane proteins. Here we present a technique for extruding gel-like LCP with embedded membrane protein microcrystals, providing a continuously-renewed source of material for serial femtosecond crystallography. Data collected from sub-10 μm -sized crystals produced with less than 0.5 mg of purified protein yield structural insights regarding cyclopamine binding to the Smoothed receptor.

Introduction

Membrane proteins constitute about one third of the proteome in most organisms, perform critical cellular and physiological functions, and represent over 60% of current drug targets in humans¹. High-resolution three-dimensional structures of membrane proteins are indispensable for understanding their functional mechanisms and designing novel drugs with high selectivity and potency. However, knowledge of membrane protein structures lags behind that of soluble proteins², emphasizing the need to develop innovative methods and approaches.

Beginning with the seminal work on photosynthetic reaction centers³, membrane proteins have historically been crystallized in detergent micelle solutions. About 15 years ago, an alternative method of crystallization was introduced, based on the use of a membrane-mimetic medium known as the lipidic cubic phase (LCP)^{4,5}. This technique has proven crucial for determining high-resolution structures and functional mechanisms of membrane proteins from several diverse families, starting with microbial rhodopsins⁶ and including G protein-coupled receptors (GPCRs), ion channels, transporters and enzymes⁷⁻¹¹.

While LCP crystallization typically produces highly ordered crystals, these crystals are often limited in size. A high density of micrometer-sized crystals in the LCP is often obtained during initial screening, but subsequent optimization to obtain sufficiently large crystals for data collection at synchrotron sources can be laborious and time consuming. Despite the fact that microcrystallography has matured over the last few years^{5,12}, structure determination of membrane proteins using microcrystals remains difficult. Ultimately, the achievable resolution for well-ordered small crystals is limited by radiation damage¹³ which poses an inherent problem for all conventional X-ray-based methods of structure determination.

LCP-grown microcrystals are ideally suited for the emerging technique of serial femtosecond crystallography (SFX)^{14,15}. SFX relies on the fact that the duration of the X-ray pulses generated by an X-ray free-electron laser (XFEL) is so brief (< 50 fs), that diffracted photons exit the sample before damage initiated by photoionization can establish itself. Diffraction is thereby recorded from essentially undamaged molecules at or close to room temperature. The peak brightness of an XFEL is a billion times higher than that of 3rd

generation synchrotrons, allowing collection of high quality single diffraction patterns from individual sub-10 μm -sized crystals in random orientations. After collecting several hundred thousand of such patterns at a rapid rate, structure factors are determined by a Monte Carlo type integration over the measured diffraction intensities¹⁶. The first experimental demonstrations of SFX, at low resolution, were carried out with membrane proteins crystallized in detergent solution¹⁷ and in the liquid-like lipidic sponge phase¹⁸. Recently, the first structures of soluble proteins in aqueous dispersion have been solved at atomic resolution^{19,20}.

To date, the SFX method has been based on X-ray data collection from a liquid stream containing protein micro/nanocrystals. The gas dynamic virtual nozzle (GDVN), which is used to inject microcrystals in their mother liquor into the X-ray beam, produces a liquid jet flowing at 10 m s^{-1} and focused to 1–5 μm diameter by employing shear and pressure forces from a co-flowing gas²¹. Hence, given the 120 Hz X-ray pulse repetition rate of the Linac Coherent Light Source (LCLS), the sample stream advances several centimeters between X-ray pulses, which are focused to 0.1–2 μm diameter. Consequently, in a typical SFX experiment, only 1 out of 10,000 microcrystals is probed by the X-ray beam. With a liquid flow rate of $10\ \mu\text{L min}^{-1}$, it takes 5–6 hours to collect a full data set, thus requiring 10–100 mg of pure protein. Obtaining such amounts is not feasible for many membrane proteins.

Because of its gel-like nature, LCP allows operation at much lower stream speeds and more efficient sample utilization. Its high viscosity, however, makes it incompatible with GDVN techniques. A new approach was needed to generate a micrometer-sized stream of LCP suitable for SFX.

We report here the development of a novel method and a device for extruding LCP at slow flow speeds and with extremely low sample consumption as a continuous 10–50 μm diameter stream. It provides a continuously renewed sample target for interrogation by the femtosecond X-ray beam. The flow speed of the injector is adjustable to the X-ray pulse repetition rate of the XFEL, so that no sample is wasted between shots. LCP-grown microcrystals of the human Smoothed receptor (SMO) in complex with cyclophamide have been injected into the femtosecond X-ray beam. Diffraction data from 61,964 microcrystals were merged to recover the structure to 3.2/4.0 \AA resolution. The protein consumption is reduced by a factor of 20 compared to SFX experiments with the GDVN nozzle.

Results and Discussion

LCP injection

The LCP micro-extrusion injector (Fig. 1) consists of a hydraulic stage, a sample reservoir and a nozzle. The reservoir can hold up to 20 μL of LCP and is connected to a fused silica capillary with 10–50 μm inner diameter (ID). The LCP is extruded out of this capillary into an evacuated sample chamber and requires a pressure of 2,000–10,000 psi, depending on the nozzle diameter and flow speed. This is provided by the hydraulic stage, which amplifies the applied pressure by a factor of 34. Shear force exerted by a co-flowing gas (helium or nitrogen at 300–500 psi supply pressure) keeps the LCP stream on axis (see methods for details).

The LCP flow-rate (typically 1–300 nL min⁻¹) depends on the sample composition, nozzle diameter and pressure and can be optimized for the 120 Hz pulse rate of the LCLS, so that between X-ray pulses the stream advances only the distance needed to expose fresh sample to the next pulse, dramatically reducing sample consumption compared to GDVN injection (Supplementary Movie 1).

The most commonly used lipid for crystallization of membrane proteins in LCP is monoolein, 9.9 MAG (an N.T MAG shorthand notation is used for monounsaturated monoacylglycerol lipids, where ‘N’ is the number of carbon atoms in the acyl chain between the ester and *cis*-olefinic bonds, and ‘T’ is the number of carbon atoms between the *cis*-olefinic bond and the end of the chain). However, this lipid is not ideally suited for the LCP-SFX experiments, as it undergoes a phase transition from the cubic phase to a lamellar crystalline (L_c) phase at 18 °C. As LCP is injected into an evacuated sample chamber at ~10⁻³ Torr and 20 °C, evaporative cooling can transform it into the L_c phase, leading to strong, sharp diffraction rings from the L_c phase (Fig. 2a). This dramatically increases the background and poses a danger to the detector, which made it necessary to attenuate the LCLS beam by a factor of 20–30. Nonetheless, in our initial experiments both microcrystal samples of β₂ adrenergic receptor (β₂AR) and adenosine A_{2A} receptor A_{2A}AR showed consistent diffraction to ~2.5 Å, even with the highly attenuated beam (Fig. 2a).

By changing the co-flowing gas from He to N₂ the formation of the L_c phase was suppressed but not completely eliminated in the case of LCP prepared with 9.9 MAG (Fig. 2c,d). However, by replacing the 9.9 MAG with shorter chain MAGs (7.9 MAG²² or 9.7 MAG (monopalmitolein) available from Avanti Polar Lipids), the formation of the L_c phase was completely prevented. Diffraction patterns collected at the LCLS confirmed the presence of the expected cubic-Pn3m phase, without a trace of the L_c phase (Fig. 2b). Additionally, we have established that for crystals that only grow in 9.9 MAG LCP (the most successful crystallization host lipid to date), 7.9 MAG can be added post crystal growth to prevent formation of the L_c phase upon injection (see Methods for details), which greatly expands the range of proteins amenable to this method. The high quality of the X-ray diffraction data collected from crystals grown in 9.9 MAG that were delivered in the 7.9/9.9 MAG mixture (Fig. 2b) shows that the crystals do not suffer from the addition of 7.9 MAG.

Diffraction Data and Sample consumption

Using the LCP injector with a flow rate of 170 nL/min, SFX data were acquired for several GPCRs, including β₂AR, A_{2A}AR, SMO, glucagon receptor and serotonin 2B (5-HT_{2B}) receptor²³, as well as the membrane enzyme diacylglycerol kinase (DgkA). Full data sets for SFX structure determination were collected for DgkA, SMO and 5-HT_{2B} over the course of 5–10 hours, while using less than 100 μL of each sample (<0.5 mg of protein). This is a vast improvement over typical sample consumption with a GDVN nozzle which requires 10 mL (10 mg protein) for a complete dataset¹⁷. A comparison of the amounts of sample used in different experiments with the GDVN and the LCP injector is included in Supplementary Table 1.

As proof of principle for the newly developed LCP-SFX method, we analyzed the data collected on human SMO receptor in complex with the naturally-occurring teratogen

cyclopamine. SMO belongs to the class Frizzled of G protein-coupled receptor superfamily, and participates in embryonic development and tumor growth. The first SMO structure in complex with an antagonist LY2940680 was recently determined by traditional microcrystallography at a synchrotron source²⁴. We were, however, unsuccessful in solving the structure of the SMO/cyclopamine complex using synchrotron data collected with a 10 μm diameter X-ray beam due to poor diffraction from relatively large crystals ($\sim 120 \times 10 \times 5 \mu\text{m}^3$; Supplementary Figure 1c,d), which presumably suffered from accumulation of crystal growth defects or from effects related to cryocooling. The LCP-SFX data collected on sub-5 μm -sized crystals (Supplementary Figure 1a,b) at room temperature were of a reasonable quality to solve the structure by molecular replacement after application of an anisotropic data truncation at 3.4, 3.2 and 4.0 \AA along three principal crystal axes (Table 1). Although the resolution is not very high, it does allow us to confidently locate where this small molecule ligand with an antitumor therapeutic potential²⁵ binds (Fig. 3). This crystallographic model will be further refined by subsequent biochemical studies.

In summary, our successful development of an LCP micro-extrusion injector allows the beneficial attributes of SFX measurements to be coupled with the unique properties and advantages of LCP for membrane protein crystallization. The new technology not only enables the collection of high-resolution structure data from LCP-grown membrane protein microcrystals at room temperature, but also dramatically reduces the amount of protein required, eliminates the need for laborious crystal size optimization, and simplifies crystal handling procedures.

Methods

LCP Injector

The LCP injector, consisting of a hydraulic stage, a sample reservoir and a nozzle, is mounted onto the end of the nozzle rod of an injector designed for XFELs²⁶. The nozzle rod can be removed from the vacuum chamber without compromising the vacuum, allowing for sample reloading and nozzle change. The hydraulic stage consists of a syringe body with a sealed solid plunger. The syringe body has a large bore on the inlet side and a much smaller bore on the outlet side. The ratio of the respective bore areas gives a nominal amplification factor of 34, delivering 10,200 psi to the LCP reservoir when water on the inlet side is pressurized to 300 psi.

The large bore in the syringe body has a diameter of 8 mm. The plunger sliding in this bore has two grooves which accept high pressure hydraulic seals (Trelleborg Turcon Variseal) and has a diameter of 8 mm on the water side and an extension with a diameter of 1.37 mm on the LCP side. The plunger extension drives two Teflon beads (Bal-tec) of 1.59 mm outer diameter, which slide in the precision bored 1.37 mm diameter LCP reservoir bore (Fig. 1). The nominal pressure amplification (neglecting frictional forces on the seals) is 34, the ratio of the squared diameters of the bores $(8 \text{ mm})^2 (1.37 \text{ mm})^{-2}$. The Teflon beads seal the bore of the reservoir against LCP leakage. When the beads are pressed into the slightly smaller reservoir bore, they deform cylindrically. The pressure applied by the plunger deforms them further and thus provides a tight seal for pressures up to 10,000 psi on the LCP.

The 360 μm outer diameter and 10–50 μm inner diameter fused silica capillary tubing (Polymicro) is kept as short as possible (6 cm) to reduce the pressure necessary to extrude the LCP. The nozzle section and the capillary are connected to the reservoir via standard HPLC conical ports (Upchurch with 10–32 threads). The tapered end of the inner capillary is inserted into a flame-polished square outer glass tube and protrudes out of the exit aperture, so that gas can flow through the open corners at a rate adequate for LCP extrusion (for details of nozzle design, see ref. ²⁶). The reservoir bore is filled with LCP via a Hamilton syringe and can hold a volume of 20 μL . The Teflon beads are replaced during each sample refill. It is possible to drive the LCP flow in a “constant pressure” mode via pressurized water connected to the plunger inlet. The supply reservoir for the water is, in turn, pressurized by gas from a gas cylinder and the LCP flow rate is controlled by adjusting the gas pressure. However, in this mode of operation the LCP flow rate would occasionally show sudden jumps (possibly due to wall stick-slip²⁷ of the LCP), leading to sample loss. Better control over LCP flow was achieved in a “constant flow-rate” mode implemented by using a HPLC pump (Shimadzu LC-20AD) to drive the hydraulic liquid (water).

The LCP flow-rate can be optimized for the 120 Hz pulse rate of the LCLS, so that between X-ray pulses the stream advances only the distance needed to expose fresh sample to the next pulse (Supplementary Movie 1). The necessary distance (the “damage diameter”) depends on the X-ray beam diameter and pulse energy. Thus, for example, at an X-ray energy of 9.5 keV, a pulse energy of 50 μJ at the sample and a beam diameter of 1.5 μm , this distance is 10–30 μm . Consequently, for a flow speed where the LCP stream travels 10–30 μm between X-ray pulses (1.2–3.6 mm s^{-1}), little if any sample is wasted and sample consumption is reduced dramatically compared to GDVN injection. Constant LCP flow-rates of 1–300 nL min^{-1} were achieved by adjusting the flow-rate setting on the HPLC pump or by using constant pressure mode (for the lowest flow rates). The minimum usable flow rate is set by the diameter of the LCP stream, the distance that the stream must advance between XFEL pulses, and the X-ray pulse repetition rate (e.g. for 120 Hz repetition rate, LCP stream diameter of 15 μm and damage diameter of 20 μm , the minimum usable flow rate is 25 nL/min .) The LCP flow-rate can be calculated by dividing the HPLC pump flow-rate by the pressure amplification factor 34.

GPCR expression and purification

Purified GPCR samples ($\beta_2\text{AR}$, $\text{A}_{2\text{A}}\text{AR}$, glucagon receptor, and 5-HT_{2B})^{24,28–31} were prepared as follows. Constructs engineered for crystallization were expressed in Sf9 insect cells for 48 h at 27 °C using recombinant baculovirus. Cells were harvested and total membranes were purified by repeated Dounce homogenization and centrifugation in hypotonic and hypertonic buffer. GPCR-ligand complexes were subsequently formed by incubating purified membranes in the presence of ligand, followed by extraction of the complexes in 1% (w/v) n-dodecyl- β -D-maltopyranoside (DDM, Anatrace) and 0.2% (w/v) cholesteryl hemisuccinate (CHS, Sigma). Solubilized proteins were purified by immobilized metal affinity chromatography (IMAC) and concentrated to ~20 – 50 mg/mL .

GPCR crystallization

Purified protein was reconstituted into LCP by mixing protein solution with molten monoolein (9.9 MAG)/10% (w/w) cholesterol at a volume ratio 2/3 (protein:lipid) using a syringe mixer³². Initial crystallization screening was performed using an NT8-LCP robot (Formulatrix) dispensing 40 nL of protein-laden LCP and overlaying it with 800 nL precipitant solution in each well of a 96-well glass sandwich plate (Marienfeld). Plates were stored at 20 °C and periodically imaged in an incubator/imager RockImager 1000 (Formulatrix). Several conditions producing high density of small crystals within 24 h were selected for scaling up (supplementary Figure 1a, b).

Crystals for LCP-SFX were obtained in Hamilton gas-tight syringes by injecting approximately 5 µL of protein-laden LCP as a continuous column of ~400 µm in diameter into a 100 µL syringe filled with 60 µL of precipitant solution and incubated for at least 24 h at 20 °C. After crystal formation and removal of excess precipitant solution, ~3 µL of molten 7.9 MAG lipid²² were added to absorb the residual precipitant solution and prevent formation of L_c phase upon injection of LCP into vacuum. The resulting crystal containing LCP sample (~10 µL) was inspected under visual and UV-microscopes as well as SONICC³³ at the LCLS and loaded in the LCP injector for LCP-SFX data collection. Samples with high crystal density were further diluted 2 times with LCP prepared from 1:1 ratio of 7.9 MAG and corresponding precipitant solution.

Smoothened receptor

An engineered human Smoothened receptor construct with truncated N-terminal cysteine-rich domain (CRD, residues 1-189) and C-terminus at Q555, and a thermostabilized *E. coli* apocytochrome B562 (BRIL)³⁴ fused into intracellular loop 3 (ICL3, replacing residues from P434 to K440) was generated, expressed and purified as described in the GPCR expression and purification section. The CRD-SMO-BRIL- C construct in complex with cyclopamine readily produced high density microcrystals in LCP following the crystallization protocol described in the GPCR crystallization section using a variety of precipitant conditions, including 100 mM Hepes pH 7.0, 30 % (v/v) PEG 400, 100 mM salt (Supplemental Fig. 1a,b). After several rounds of optimization, relatively large crystals obtained in conditions with ammonium salts (Supplementary Fig. 1c,d) were used for data collection at a synchrotron source, and microcrystals obtained in 100 mM Hepes pH 7.0, 30 % (v/v) PEG 400, 100 mM NaCl were used for LCP-SFX data collection.

DgkA expression and purification

The coding sequence of a thermostable mutant variant of DgkA, with its N-terminal methionine replaced by a hexa-His tag-containing decapeptide (MGHHHHHHEL) to facilitate purification, was synthesized and cloned¹⁰. This mutant, referred to as 7 DgkA, incorporated seven mutations with respect to wild type DgkA, as follows: A41C, C46A, I53V, I70L, M96L, V107D, and C113A. DgkA production and purification, primarily from inclusion bodies, were carried out following published procedures¹⁰.

DgkA crystallization

Crystallization trials began with the reconstitution of the protein into the bilayer of the lipidic cubic mesophase following a standard protocol³². The protein solution at 12 mg/mL was homogenized with 7.9 MAG in equal parts by volume using a coupled syringe device at room temperature (20–22 °C). Approximately 20 μ L of protein-laden mesophase was transferred into a 0.5 mL Hamilton syringe containing 0.4 mL precipitant solution (0.2 % (v/v) MPD, 0.1 M sodium chloride, 0.1 M sodium citrate pH 5.6) using a narrow bore coupler³², as described above for GPCR crystallization. The syringe was incubated for 21 d at 20 °C for crystal growth. After separating the bathing solution from the crystal-laden LCP, excess precipitant was absorbed by mixing in 3–5 μ L molten 7.9 MAG. This procedure produced optically clear LCP in which microcrystals were dispersed ready for loading into the reservoir of the LCP injector, as described above.

Experimental setup at LCLS and data acquisition rates

The experiment took place at the LCLS in the sample chamber of the Coherent X-ray Imaging (CXI) instrument³⁵, using 9.5 keV (1.3 Å) X-ray pulses with a pulse length of 50 fs and repetition rate of 1–120 Hz. The pressure in the experimental chamber was $\sim 10^{-5}$ Torr; the pressure at the extruded LCP sample was about $10^{-1} - 10^{-3}$ Torr depending on the gas flow rate of the sheath gas. The nozzle area is pumped by a differential pumping system, which reduces gas flow from the nozzle into the main chamber²⁶. Due to evaporative cooling, the sample temperature at the point of the X-ray interaction (100 μ m downstream of the nozzle exit) is estimated to be slightly below room temperature. An XFEL beam diameter of 1.5 μ m was used. With an LCLS frequency of 60–120 Hz (depending on the LCP flow rate), one million diffraction patterns, which is a sufficiently large data set to achieve atomic resolution, can be collected in ~ 2.5 hours with 25 μ L of sample.

LCP-SFX data for SMO/cyclopamine crystals were collected at an X-ray pulse repetition rate of 120 Hz. The sample-to-detector distance was 100 mm and the beam was attenuated to 3–6 % ($2.5-5 \cdot 10^{10}$ photons/pulse) of the full intensity to avoid detector saturation. A total of 3,510,525 diffraction patterns were collected, of which 274,214 were identified as potential single crystal diffraction patterns with more than 15 potential Bragg peaks by the software Cheetah³⁶, corresponding to an average hit rate of 7.8 %. Autoindexing and structure factor integration of the crystal hits was performed using CrystFEL (version 0.5.1)³⁷, resulting in 61,964 indexed images with a monoclinic lattice (22.6% indexing success rate). Based on the observation of systematic absences (Supplementary Fig. 2) and the behavior of the Pearson correlation coefficient (Supplementary Fig. 3), we concluded that the diffraction data reach about 3 Å resolution, but are highly anisotropic. The UCLA anisotropy server (<http://services.mbi.ucla.edu/anisoscale/>) was used to truncate data at 3.4, 3.2 and 4.0 Å resolution along the three principal axes. Data collection statistics are summarized in Table 1.

Structure determination and refinement

The SMO/cyclopamine structure was determined by molecular replacement with the program Phaser³⁸ using the receptor domain of the previously reported SMO structure in complex with LY2940680 (PDB ID: 4JKV) and the BRIL domain from 5-HT_{2B} structure

(PDB ID: 4IB4) as the search models. After several rounds of alternate refinement by Phenix.refine³⁹, including simulated annealing to remove phase bias, and manual inspection and corrections in Coot⁴⁰ in the absence of any ligand, extra electron density was observed in the same vicinity of the LY2940680 ligand binding site (Fig. 3). Due to the limited diffraction resolution and a relatively featureless shape of cyclopamine, orienting this ligand in the available elongated density was not straightforward and required combining additional information based on chemical knowledge to create a reasonable model. Since it has been reported that cyclopamine derivatives with bulky substitution groups attached to its secondary amine retain their ability to bind SMO^{25,41}, cyclopamine was placed in the density with its secondary amine group pointing to the open extracellular space needed to accommodate bulky substitutions. After aligning the major axis of cyclopamine, two alternative orientations of cyclopamine differing by about 180° rotation around its major axis could still be placed in the available electron density. One of these orientations was selected for further refinement based on the favorable conformer energy for cyclopamine, although the second orientation could not be entirely ruled out. The obtained model containing cyclopamine was further refined resulting in $R_{\text{work}}/R_{\text{free}} = 0.232/0.278$ (Table 1). The structure has an excellent geometry according to the MolProbity server⁴² with 95.6% residues in the favored and 4.4% residues in the allowed Ramachandran conformations. Residues 345-354 (intracellular loop 2) and 497-504 (extracellular loop 3) were not modeled due to poor density in these regions.

Supplementary Material

Refer to Web version on PubMed Central for supplementary material.

Acknowledgments

Experiments were carried out at the Linac Coherent Light Source, a national user facility operated by Stanford University on behalf of the U.S. Department of Energy (DOE), Office of Basic Energy Sciences. The work was supported in part by the National Institutes of Health Common Fund in Structural Biology grants P50 GM073197 (V.C. and R.C.S.), P50 GM073210 (M.C.), R01 GM095583 (P.F.), and NIGMS PSI:Biological grants U54 GM094618 (V.C. and R.C.S.), U54 GM094599 (P.F.), U54 GM094625 (M.C.). We acknowledge support from the National Science Foundation (awards MCB 1021557 and MCB 1120997) (J.C.H.S, U.W., P.F., R.B.D.) and its BioXFEL Science and Technology Center (NSF 1231306) and the Science Foundation Ireland (12/IA/1255). We further acknowledge support from the Helmholtz Gesellschaft and the Max Planck Gesellschaft (R.L.S). Special thanks to T. Trinh and M. Chu for help with baculovirus expression, F. Siu for help with sample preparation, and A. Walker for assistance with manuscript preparation. We are grateful to Richard Flubacher and the machinists of the ASU Mechanical Instrument Shop for their skill in fabricating injector components.

References

1. Yildirim MA, Goh KI, Cusick ME, Barabási AL, Vidal M. Drug-target network. *Nat Biotechnol.* 2007; 25:1119–1126. [PubMed: 17921997]
2. White SH. The progress of membrane protein structure determination. *Protein Sci.* 2004; 13:1948–1949. [PubMed: 15215534]
3. Deisenhofer J, Epp O, Miki K, Huber R, Michel H. Structure of the protein subunits in the photosynthetic reaction centre of *Rhodospseudomonas viridis* at 3 Å resolution. *Nature.* 1985; 318:618–624. [PubMed: 22439175]
4. Cherezov V, et al. Rastering strategy for screening and centring of microcrystal samples of human membrane proteins with a sub-10 µm size X-ray synchrotron beam. *J R Soc Interface.* 2009; 6:S587–S597. [PubMed: 19535414]

5. Landau EM, Rosenbusch JP. Lipidic cubic phases: a novel concept for the crystallization of membrane proteins. *P Natl Acad Sci USA*. 1996; 93:14532–14535.
6. Pebay-Peyroula E. X-ray Structure of Bacteriorhodopsin at 2.5 Angstroms from Microcrystals Grown in Lipidic Cubic Phases. *Science*. 1997; 277:1676–1681. [PubMed: 9287223]
7. Cherezov V, et al. High-Resolution Crystal Structure of an Engineered Human 2-Adrenergic G Protein Coupled Receptor. *Science*. 2007; 318:1258. [PubMed: 17962520]
8. Santos JS, et al. Crystal Structure of a Voltage-gated K⁺ Channel Pore Module in a Closed State in Lipid Membranes. *J Biol Chem*. 2012; 287:43063–43070. [PubMed: 23095758]
9. Liao J, et al. Structural Insight into the Ion-Exchange Mechanism of the Sodium/Calcium Exchanger. *Science*. 2012; 335:686–690. [PubMed: 22323814]
10. Li D, et al. Crystal structure of the integral membrane diacylglycerol kinase. *Nature*. 2013; 497:521–524. [PubMed: 23676677]
11. Cherezov V. Lipidic cubic phase technologies for membrane protein structural studies. *Curr Opin Struc Biol*. 2011; 21:559–566.
12. Smith JL, Fischetti RF, Yamamoto M. Micro-crystallography comes of age. *Curr Opin Struc Biol*. 2012; 22:602–612.
13. Garman EF. Radiation damage in macromolecular crystallography: what is it and why should we care? *Acta Cryst D*. 2010; 66:339–351. [PubMed: 20382986]
14. Spence J, Weierstall U, Chapman H. X-ray lasers for structural and dynamic biology. *Rep Prog Phys*. 2012; 75:102601. [PubMed: 22975810]
15. Fromme P, Spence JC. Femtosecond nanocrystallography using X-ray lasers for membrane protein structure determination. *Curr Opin Struc Biol*. 2011; 21:509–516.
16. Spence JCH, et al. Phasing of coherent femtosecond X-ray diffraction from size-varying nanocrystals. *Opt Express*. 2011; 19:2866. [PubMed: 21369108]
17. Chapman HN, et al. Femtosecond X-ray protein nanocrystallography. *Nature*. 2011; 470:73–77. [PubMed: 21293373]
18. Johansson LC, et al. Lipidic phase membrane protein serial femtosecond crystallography. *Nat Meth*. 2012; 9:263–265.
19. Boutet S, et al. High-resolution protein structure determination by serial femtosecond crystallography. *Science*. 2012; 337:362–364. [PubMed: 22653729]
20. Redecke L, et al. Natively Inhibited Trypanosoma brucei Cathepsin B Structure Determined by Using an X-ray Laser. *Science*. 2013; 339:227–230. [PubMed: 23196907]
21. DePonte DP, et al. Gas dynamic virtual nozzle for generation of microscopic droplet streams. *J Phys D Appl Phys*. 2008; 41:195505.
22. Misquitta Y, et al. Rational design of lipid for membrane protein crystallization. *J Struct Biol*. 2004; 148:169–175. [PubMed: 15477097]
23. Liu W, et al. Serial Femtosecond Crystallography of G Protein-Coupled Receptors. *Science*. 2013; 342:1521–1524. [PubMed: 24357322]
24. Wang C, et al. Structure of the human smoothed receptor bound to an antitumour agent. *Nature*. 2013; 497:338–343. [PubMed: 23636324]
25. Taipale J, et al. Effects of oncogenic mutations in Smoothed and Patched can be reversed by cyclopamine. *Nature*. 2000; 406:1005–1009. [PubMed: 10984056]
26. Weierstall U, Spence JCH, Doak RB. Injector for scattering measurements on fully solvated biospecies. *Rev Sci Instrum*. 2012; 83:035108–035108. [PubMed: 22462961]
27. Hatzikiriakos SG. Wall slip of molten polymers. *Progress in Polymer Science*. 2012; 37:624–643.
28. Hanson MA, et al. A Specific Cholesterol Binding Site Is Established by the 2.8 Å Structure of the Human β₂-Adrenergic Receptor. *Structure*. 2008; 16:897–905. [PubMed: 18547522]
29. Liu W, et al. Structural basis for allosteric regulation of GPCRs by sodium ions. *Science*. 2012; 337:232–236. [PubMed: 22798613]
30. Wacker D, et al. Structural Features for Functional Selectivity at Serotonin Receptors. *Science*. 2013; 340:615–619. [PubMed: 23519215]
31. Siu FY, et al. Structure of the human glucagon class B G-protein-coupled receptor. *Nature*. 2013; 499:444–449. [PubMed: 23863937]

32. Caffrey M, Cherezov V. Crystallizing membrane proteins using lipidic mesophases. *Nat Protoc.* 2009; 4:706–731. [PubMed: 19390528]
33. Kissick DJ, Gualtieri EJ, Simpson GJ, Cherezov V. Nonlinear Optical Imaging of Integral Membrane Protein Crystals in Lipidic Mesophases. *Anal Chem.* 2010; 82:491. [PubMed: 20025250]
34. Chun E, et al. Fusion Partner Toolchest for the Stabilization and Crystallization of G Protein-Coupled Receptors. *Structure.* 2012; 20:967–976. [PubMed: 22681902]
35. Boutet S, Williams GJ. The Coherent X-ray Imaging (CXI) instrument at the Linac Coherent Light Source (LCLS). *New J Phys.* 2010; 12:035024.
36. White TA, et al. Crystallographic data processing for free-electron laser sources. *Acta Cryst D.* 2013; 69:1231–1240. [PubMed: 23793149]
37. White TA, et al. CrystFEL: a software suite for snapshot serial crystallography. *J Appl Crystallogr.* 2012; 45:335–341.
38. McCoy AJ, et al. Phaser crystallographic software. *J Appl Crystallogr.* 2007; 40:658–674. [PubMed: 19461840]
39. Adams PD, et al. PHENIX: a comprehensive Python-based system for macromolecular structure solution. *Acta Cryst D.* 2010; 66:213–221. [PubMed: 20124702]
40. Emsley P, Lohkamp B, Scott WG, Cowtan K. Features and development of Coot. *Acta Cryst D.* 2010; 66:486–501. [PubMed: 20383002]
41. Chen JK, Taipale J, Cooper MK, Beachy PA. Inhibition of Hedgehog signaling by direct binding of cyclopamine to Smoothened. *Genes Dev.* 2002; 16:2743–2748. [PubMed: 12414725]
42. Chen VB, et al. MolProbity: all-atom structure validation for macromolecular crystallography. *Acta Cryst D.* 2009; 66:12–21. [PubMed: 20057044]

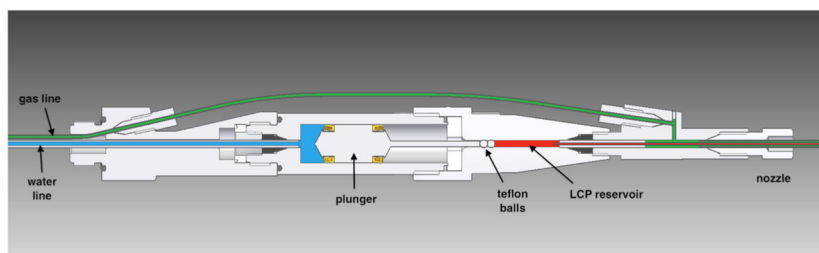


Fig. 1. Middle section through the LCP injector

In operation, the device is attached via the leftmost threaded fitting to a nozzle rod (not shown) for insertion into the experimental chamber. Water (blue) and gas (green) lines are routed through the nozzle rod from the left, LCP (red) is extruded from the nozzle on the right. Water, at a pressure of up to 300 psi, drives the hydraulic plunger, which amplifies the pressure 34 times to drive LCP through a capillary with an inner diameter of 10–50 μm . Two spherical Teflon beads are used to provide a tight seal against a pressure of up to 10,000 psi. The co-flowing gas is necessary for reliable extrusion and to maintain co-axial flow.

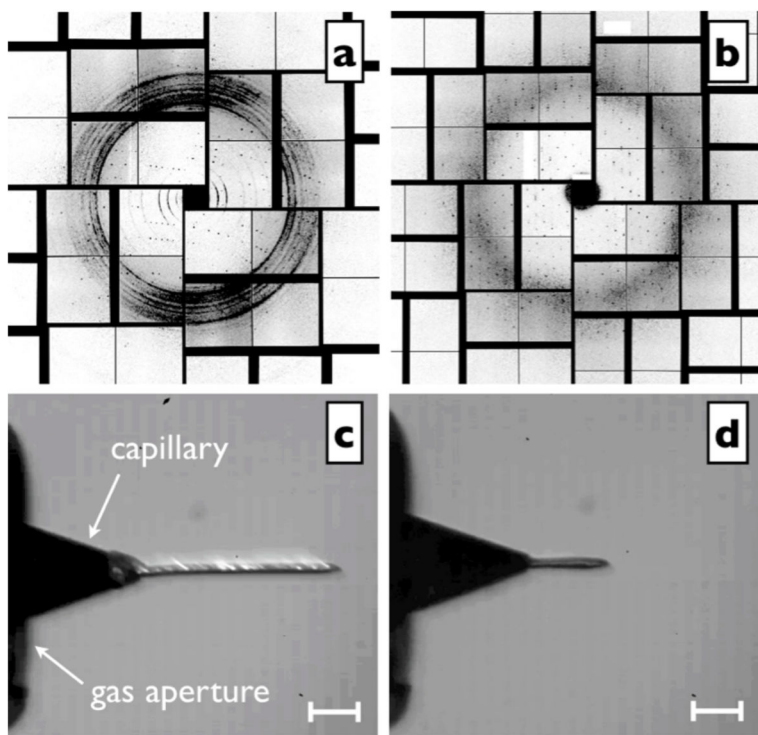


Fig. 2. Snapshot diffraction patterns and LCP extrusion

Panels (a) and (b): Single femtosecond snapshot diffraction patterns. (a) Diffraction spots from A_{2A} adenosine receptor microcrystals in 9.9 MAG/cholesterol LCP to 2.5 Å and strong powder diffraction rings from crystalline lipid. (X-ray intensity attenuated to 7%, 1.5 μm X-ray beam diameter, 50 fs pulse length, 9.5 keV, 15 μm LCP jet diameter, 300 pL/min flow rate, 1 Hz pulse rate, crystal size: 1×1×5 μm³). (b) Diffraction from serotonin receptor 5-HT_{2B} in cholesterol-doped 9.9 MAG + 7.9 MAG LCP. No sharp rings are visible suggesting that formation of L_c phase has been avoided (X-ray intensity attenuated to 3.1% due to strong Bragg diffraction from 5×5×5 μm³ sized crystals, 1.5 μm X-ray beam diameter, 50 fs pulse length, 9.5 keV, 50 μm LCP jet diameter, 190 nL/min flow rate, 120 Hz pulse rate). The resolution at the detector edge in both panels is 2.5 Å. Panels (c) and (d): 9.9 MAG LCP extrusion in vacuum viewed between crossed polarizers. The tapered end of the capillary nozzle is seen protruding out of the gas aperture. Capillary inner diameter: 30 μm. (c) with He as co-flowing gas. Birefringence (bright flecks) is an indication of a transition of the cubic phase to a lamellar crystalline phase due to evaporative cooling. (d) with N₂ as co-flowing gas and no visible birefringence. Scale bars: 100 μm.

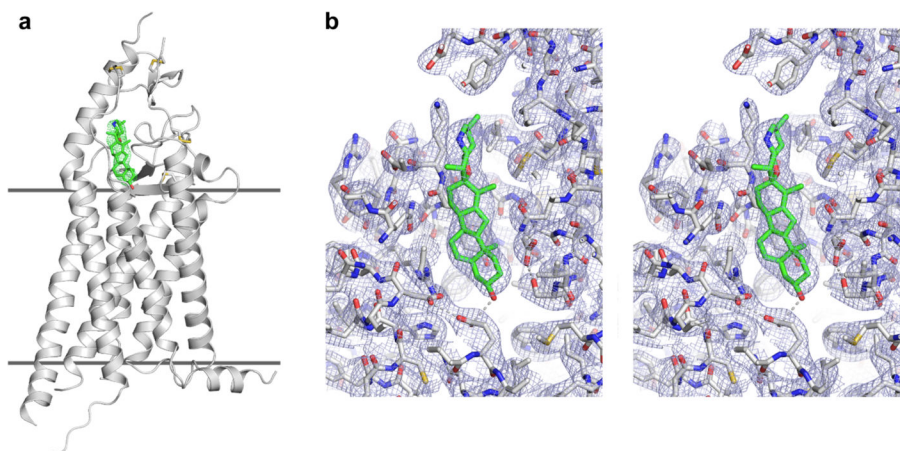


Fig. 3. Cyclopamine binding to Smoothened receptor

(a) Receptor model is shown as a gray cartoon, cyclopamine as a stick model with green carbons, and the “omit” $2mF_o-DF_c$ density map for cyclopamine contoured at 1σ is shown as green wires. Horizontal lines indicate membrane boundaries. (b) Cyclopamine binding pocket is shown in stereo view as a stick model along with $2mF_o-DF_c$ density map contoured at 1σ . Cyclopamine binds near to the entrance into a long and narrow cavity inside the receptor. Polar interactions stabilizing the shape of the cavity and cyclopamine binding are shown as gray dashed lines. Viewing angles in (a) and (b) are slightly different.

Table 1

Data collection and refinement statistics.

	SMO/cycloamine
Data collection	
Space group	P2 ₁
Cell dimensions,	
a, b, c (Å)	40.5, 157.3, 52.4
α, β, γ (°)	90.0, 97.0, 90.0
Resolution (Å)	40 – 3.20 (3.26 – 3.20) [#]
R _{split} (%)	9.8 (63.2)
I/σ(I)	7.4 (1.8)
CC*	0.9991 (0.28)
Completeness (%)	100 (100)
Multiplicity	2,515 (1,820)
Refinement	
Resolution (Å)	40 – 3.20
Anisotropic truncation (Å)	3.4, 3.2, 4.0
No. reflections/test set	8,082/399
R _{work} /R _{free}	0.232/0.278
No. atoms	
Protein	3,389
Cycloamine	30
B-factors (Å ²)	
Wilson B/Overall B	101.6/78.4
Receptor/BRIL	76.8/83.7
Cycloamine	76.3
R.m.s deviations	
Bonds lengths(Å)	0.003
Bond angles (°)	0.61

[#]High resolution shell is shown in parentheses

This dataset includes diffraction from 61,964 crystals